Research Square

Preprints are preliminary reports that have not undergone peer review.
They should not be considered conclusive, used to inform clinical practice,
or referenced by the media as validated information.

SAS-6 coordinates cell-matrix and cell-cell interactions to promote cancer cell migration

Rebecca Collinson
Brunel University of London
Zoi Grigoriou-Mirallais
Brunel University of London
Elizabeth McCarthy
Brunel University of London
Joseph Hetmanski
Brunel University of London
Barbara Eugenia Tanos
barbara.tanos@brunel.ac.uk

Brunel University of London

Article

Keywords: SAS-6, centrioles, cell migration, extracellular matrix, cell junctions, lung cancer

Posted Date: November 5th, 2026

DOI: https://doi.org/10.21203/rs.3.rs-11360807/v1

License: This work is licensed under a Creative Commons Attribution 4.0 International License.
Read Full License

Additional Declarations: No competing interests reported.

Abstract

Background

The ability of cancer cells to migrate is essential for metastatic progression. Centrioles regulate cytoskeleton remodelling and cell polarity, two key stages of migration, whilst centrosome amplification is commonly observed in aggressive cancer types. Spindle assembly abnormal protein 6 homolog (SAS-6) is a central component of centrioles required for normal duplication and function. To understand further how centrioles could affect cell migration, here we investigated the effects of depleting and overexpressing SAS-6 on cell morphology and movement in physiologically relevant cell derived matrices (CDMs).

Methods

SAS-6 levels were depleted in a metastatic small cell lung cancer cell line using shRNA-mediated gene knockdown. The effects of overexpression of a non-degradable form of SAS-6 were also investigated. The biological significance of SAS-6 perturbation on cell migration was investigated using live cell imaging. Actin organisation, cell junction formation, and cell membrane dynamics were analysed using immunofluorescence and open-source computational software.

Results

A metastatic small cell lung cancer cell line was characterised upon SAS-6 depletion, which was found to reduce centriole amplification and cilia number. Depletion of SAS-6 reduced cell migration in CDMs, whilst SAS-6 overexpression increased migration speed and distance. SAS-6 depletion increased focal adhesion number and size, altered actin organisation, disrupted cell anterior-posterior polarity, and weakened cell-cell contacts.

Conclusions

This study shows a role for the centriolar protein SAS-6 in the regulation of cell migration, likely through coordinating cellular interactions with the surrounding matrix and neighbouring cells, as well as regulating anterior-posterior polarity during cell movement. These observations provide strong rationale to explore SAS-6 as a therapeutic target in cancer metastasis.

Introduction

Centrosomes are the primary microtubule-organising centre (MTOC) in most mammalian cells. They coordinate proper mitotic spindle assembly and chromosome segregation, thereby regulating correct cell division. Centrosomes are also involved in maintaining correct cell polarity, necessary for cell

migration (Ueda *et al.*, 1997, Zhang *et al.*, 2014, Zhang & Wang, 2017). Cell cycle exit triggers the maturation of the mother centriole into a basal body, an essential stage in primary cilium formation (Satir & Christensen, 2007). Primary cilia are sensory organelles that receive and transduce chemical and mechanical signals from the extracellular environment (Mill *et al.*, 2023). Given the many roles of centrioles in cell physiology, it is perhaps unsurprising that centrosomal and ciliary abnormalities are implicated in the development of a number of cancers (Godinho & Pellman, 2014, Godinho *et al.*, 2014, Jenks *et al.*, 2018, Collinson & Tanos, 2025). Centriole amplification and over-elongation are commonly observed in cancer cell lines and patient samples, as reviewed in (Marteil *et al.*, 2018), and have been shown to drive invasion and tumorigenesis (Godinho & Pellman, 2014, Godinho *et al.*, 2014, Levine *et al.*, 2017, Marteil *et al.*, 2018).

Spindle assembly abnormal protein 6 homolog (SAS-6) is a member of a group of six proteins essential for centriole duplication, assembly, and elongation (Leidel *et al.*, 2005, Delattre *et al.*, 2006, Pelletier *et al.*, 2006, Sugioka *et al.*, 2017). SAS-6 accumulates from S-phase until the end of mitosis, when its degradation is triggered by ubiquitination by APC/C-Cdh1 (Strnad *et al.*, 2007). *SASS6* has been shown to be overexpressed in colorectal cancer, oesophageal squamous carcinoma, lung adenocarcinoma and breast cancer (Lee *et al.*, 2014, Shinmura *et al.*, 2015, Xu *et al.*, 2021, Li *et al.*, 2024). We have previously shown that SAS-6 overexpression results in increased YAP/TAZ signalling, actin contractility, cell protrusion, and increased invasion through a collagen matrix (Hargreaves *et al.*, 2025). Interestingly, we also found that knocking down SAS-6 in a metastatic small cell lung cancer (SCLC) cell line with high endogenous SAS-6 expression (DMS273) resulted in an almost complete block of cell invasion (Hargreaves *et al.*, 2025).

As metastatic disease is the major cause of death in cancer patients (Dillekås *et al.*, 2019), we sought to further investigate the roles of SAS-6 in contributing to this process. Given that DMS273 is a highly ciliated cell line isolated from the metastatic spread of SCLC, it represents a valuable tool to examine this process. Interestingly, DepMap analysis showed that DMS273 has a high probability of SAS-6 dependence. shRNA-mediated downregulation of SAS-6 resulted in a significant decrease in SAS-6 localisation to centrioles and the number of ciliated cells. To understand the role of SAS-6 in migration in a physiologically relevant setting, we generated cell-derived matrices (CDMs) (Yamada & Cukierman, 2007, Appert-Collin *et al.*, 2017). SAS-6 depletion decreased migration in CDMs whilst overexpressing SAS-6 increased cell movement. SAS-6 downregulation was also found to weaken cell-cell junctions and resulted in significant changes in cell surface area, actin dynamics, focal adhesions and overall reduced velocity. DepMap analysis showed high gene co-dependency with ZO-1, a junctional protein implicated in collective cell migration. Removal of SAS-6 resulted in reduced ZO-1 protein levels and ZO-1 localisation at cell junctions, suggesting a collaborative role for SAS-6 and ZO-1 in cell migration. Together these findings suggest a role for SAS-6 in coordinating cell migration and attachment, two essential steps of cancer cell metastasis.

Methods

Cell lines and reagents

All cell lines were maintained at 37 ^{O}C in a humidified atmosphere containing 5% CO_2. Human telomerase-immortalised retinal pigment epithelial cells (hTERT-RPE-1 or RPE-1) were purchased from the ATCC and transduced with pBABE retro GFP-centrin 2. A single cell clone of RPE-1 expressing tetracycline-inducible non-degradable SAS-6 (SAS-6ND) was generated as described previously (Hargreaves *et al.*, 2025). DMS273 cells were kindly provided by Dr Igor Vivanco (King's College London). RPE-1 SAS-6ND and DMS273 cells were cultured in Dulbecco's Modified Eagle's Medium/Nutrient Mixture F-12 Ham (DMEM/F-12; Sigma-Aldrich) containing 0.365 mg/mL L-glutamine, 15 mM HEPES, 1.2 mg/mL sodium bicarbonate, and supplemented with 10% foetal bovine serum (FBS; Gibco) and 1% penicillin/streptomycin (Gibco). 1 µg/mL doxycycline (Sigma-Aldrich) was added to RPE-1 SAS-6ND growth media for 6 d before use in experiments to induce SAS-6ND expression. Telomerase-immortalised fibroblasts (TIFs) were kindly provided by Professor Patrick Caswell (University of Manchester) and were maintained in DMEM (Sigma-Aldrich) containing 0.584 mg/mL L-glutamine and supplemented with 10% FBS, and 1% antibiotic-antimycotic (Sigma-Aldrich). HEK293T cells were acquired from ATCC and maintained in high-glucose DMEM (Sigma-Aldrich) containing 4500 mg/L glucose, 0.584 mg/mL L-glutamine, and 3.7 mg/mL sodium bicarbonate, supplemented with 10% FBS and 1% penicillin/streptomycin.

Short hairpin RNA-mediated gene knockdown

To generate SAS-6 knockdown cells, a short hairpin RNA (shRNA) targeting human SASS6 in a pLKO.1 lentiviral vector (The RNAi Consortium/Horizon, Clone ID TRCN0000130315) was transiently co-transfected into HEK293T cells with packaging and envelope vectors using polyethylenimine (PEI; Polysciences) as a transfection reagent. Virus was collected and filtered before use for two sequential infections of DMS273 cells. shRNA targeting firefly luciferase (shLuc; absent in mammalian genomes) was used as a control. Stable shRNA expressors were selected with 5 µg/mL puromycin (Sigma-Aldrich) and knockdown was confirmed by western blot.

Western blots

Cells were lysed in ice-cold RIPA buffer (Thermo Fisher Scientific) supplemented with a cocktail of protease and phosphatase inhibitors (Thermo Fisher Scientific). Lysates were sonicated and cleared by centrifugation at 14,000 *g* for 10 min. Protein content was determined using the DC Protein Assay (Bio-Rad). Protein samples were diluted in 2X Laemmli sample buffer (Bio-Rad) containing b-mercaptoethanol (Sigma-Aldrich) and denatured at 95 ^{O}C for 10 min. Protein samples were separated by SDS-PAGE and transferred to a nitrocellulose membrane. Membranes were blocked in 5% milk in tris-buffered saline (Thermo Fisher Scientific) and 0.05% Tween-20 (TBST; Sigma-Aldrich) then incubated in the relevant primary and HRP-conjugated secondary antibodies (Table 1). Immunoreactivity was

revealed using SuperSignal West Pico Plus ECL (Thermo Fisher Scientific). Blots were visualised using the G:Box Chemi imager (Syngene). Image analysis was performed using FIJI.

Table 1
– Antibodies used for immunoblotting.

Target	Brand	Catalogue number	Dilution
α-tubulin	Invitrogen	A11126	1:5000
c-Myc epitope tag	Invitrogen	13-2500	1:1000
SAS-6	Santa Cruz Biotechnology	sc-81431	1:1000
Vinculin	Sigma-Aldrich	V9131	1:10000
ZO-1	Invitrogen	61-7300	1:1000
Mouse-IgG, HRP-linked	Cell Signaling Technology	7076	1:2000
Rabbit-IgG, HRP-linked	Cell Signaling Technology	7074	1:2000

Immunofluorescence

Cells were grown on 12mm, #1.5 thickness poly-L-lysine-coated coverslips (VWR) or poly-D-lysine/fibronectin-coated coverslips (Neuvitro) and fixed in 4% paraformaldehyde (PFA) for 10 min at room temperature. Cells were permeabilised for 5 min in 0.1% Triton X-100 in PBS (PBST) and blocked for 5 min in 3% BSA in PBST (PBSBT). Cells were incubated at room temperature for 1 h in the relevant primary antibodies/probes (Table 2) diluted in PBSBT. Cells were washed three times in PBST before incubation for 1 h in the relevant secondary antibodies (Table 2), followed by three PBST washes and DAPI (Thermo Fisher Scientific) staining for DNA visualisation. Coverslips were mounted onto slides with ProLong Diamond Antifade Reagent (Thermo Fisher Scientific).

Table 2
– Antibodies and labels used in immunostaining.

Target	Brand	Catalogue number	Dilution
g-tubulin	Santa Cruz Biotechnology	sc-51715	1:500
Acetylated tubulin	Sigma-Aldrich	T7451	1:2000
Arl13B	Proteintech	17711-1-AP	1:500
Centrin 3	Abnova	H00001070-M01	1:200
CP110	Proteintech	12780-1-AP	1:200
Detyrosinated tubulin	Abcam	ab48389	1:400
Fibronectin	BD Biosciences	610077	1:500
Phalloidin, Alexa Fluor 546	Invitrogen	A22283	1:100
SAS-6	Santa Cruz Biotechnology	sc-81431	1:500
Vinculin	Sigma-Aldrich	V9131	1:500
ZO-1	Invitrogen	61-7300	1:200
Mouse-IgG1, Alexa Fluor 647	Invitrogen	10789384	1:500
Mouse-IgG2b, Alexa Fluor 488	Invitrogen	10337122	1:500
Rabbit-IgG H + L, Alexa Fluor 488	Invitrogen	17177061	1:500
Rabbit-IgG H + L, Alexa Fluor 555	Invitrogen	10533433	1:500
Rabbit-IgG H + L, Alexa Fluor 594	Invitrogen	10474352	1:500

For centriole marker visualisation, cells were fixed first with 4% PFA, then in ice-cold methanol for 20 min, followed by a 2 min permeabilisation in PTEM buffer containing 20 mM PIPES (pH 6.8), 0.2% Triton X-100, 10 mM EGTA, and 1 mM $MgCl_2$. Immunostaining then continued as described above.

Cells grown in CDMs were fixed in 4% PFA for 30 min at room temperature and incubated in each antibody for 2 h at room temperature. CDMs were imaged immediately after staining as no antifade mountant was used.

Cell-derived matrix generation

Cell-derived matrices (CDMs) were generated in 6- or 12-well plates (Sarstedt) or 35 mm glass bottom plates (Mattek). Plates were coated with 0.2% gelatin (v/v; Sigma-Aldrich) for 1 h, crosslinked with 1% glutaraldehyde (v/v; Sigma-Aldrich) for 30 min, and quenched with 1 M glycine (Thermo Fisher Scientific) for 20 min. TIFs were confluently seeded into the prepared plates, and DMEM supplemented with 0.25%

ascorbic acid (v/v; Sigma-Aldrich) was changed every 48 h for 8 d. Cells were denuded with extraction buffer containing 20 mM ammonium hydroxide (NH_4OH) and 0.5% Triton X-100 to leave only matrix before treatment with 10 µg/ml DNase 1 (Roche) to cleave phosphodiester linkages in the DNA backbone. CDMs were stored at 4°C with 1% antibiotic-antimycotic (Sigma-Aldrich) and used within 3 months of generation.

Migration assay

DMS273 or RPE-1 SAS-6ND cells were seeded at sparse confluency (50,000 cells/well for 6-well plates, 20,000 cells/well for 12-well plates) onto CDMs. DMS273 were allowed to attach for 24 h before imaging, RPE-1 SAS-6ND were allowed to attach for 4 h before imaging. Phase contrast images were captured every 10 min for 16 h using a Cytation 5 (Agilent Technologies) automated cell imager through a 10X Olympus objective. Images were acquired with a Sony IMX254 CMOS camera using BioTek Gen 5 software (version 3.12).

Five positions were chosen within each well. 10 cells from each position were chosen at random (excluding cells which disappeared from the field of view over the 16 h period) and tracked using the MTrackJ FIJI plugin every 3 frames (30 min timepoint intervals) (Meijering *et al.*, 2012).

Live imaging of fluorescently labelled cells

To follow actin cytoskeleton dynamics, pLVX-LifeAct-RFP, kindly provided by the Way lab (The Francis Crick Institute), was transiently co-transfected into HEK293T cells with packaging and envelope vectors using polyethylenimine (PEI; Polysciences) as a transfection reagent. Virus was collected and filtered before use for two sequential infections of DMS273 shLuc and shSASS6 cells. Stable expressors were selected by gating for equal levels of RFP with a CytoFLEX SRT Benchtop Cell Sorter (Beckman Coulter).

Cells were seeded at sparse confluency onto CDMs and allowed to spread for 24 h. For each condition, 25 fluorescent cells were located before imaging at 2 min intervals for a total of 1 h at 37 ^{o}C and 5% CO_2. Analyses of membrane protrusions were performed using the ADAPT plugin in ImageJ (Barry *et al.*, 2015).

Fluorescence image acquisition, processing, and analysis

Fluorescence images were acquired on an upright Axio Imager M2 microscope (Zeiss) equipped with 100X and 40X oil objectives, 1.4 numerical aperture, an ORCA R2 camera (Hamamatsu Photonics) and a computer with ZenPro image processing software (Zeiss).

Confocal fluorescence images were acquired using a fully motorised Nikon Ti2 inverted microscope stand, fitted with a Prior Scientific NanoScan SP600 piezo insert. The microscope stand was equipped with a Crest Optics X-light V3 spinning disk (50 mm pinhole size) confocal unit. Images were captured

using a Teledyne Photometrics Kinetix camera through 40X, 60X and 100X objectives. Data were acquired in the NIS Elements AR software (version 6.10.02) and saved in the ND2 file format.

Images were processed using ImageJ/FIJI and figures were assembled in Illustrator (Adobe). Intensity and morphology quantifications were performed with CellProfiler (Stirling *et al.*, 2021). Scale bars are indicated in each figure.

DepMap analyses

Gene expression and dependency data was acquired from the DepMap Public 26Q1 Dataset (https://depmap.org/portal) (Arafeh *et al.*, 2025).

RNA expression (short-read, log2[TPM + 1]) was compared with gene dependency scores derived from a genome-wide CRISPR/Cas9 knockout screen using the DepMap Data Explorer 2.0.

The depmap_predictability_data_SASS6 dataset containing data from the CRISPR (DepMap Public 26Q1 + Score, Chronos) and RNAi (Achilles+DRIVE+Marcotte, DEMETER2) screens was downloaded and used to map SAS-6 dependence predictability. Only expression data were incorporated in this analysis. Relative gene importance was plotted against the Pearson's correlation coefficient.

BioGRID data

Protein interaction data for SAS-6 was obtained from the Biological General Repository for Interaction Datasets (BioGRID) (Oughtred *et al.*, 2021).

Statistical analysis

Statistical analyses were performed with GraphPad Prism. Statistical tests are specified in the figure legends.

Results

Characterisation of a ciliated metastatic cancer cell line to study cell migration

DMS273 is a metastatic human small cell lung carcinoma (SCLC) cell line isolated from the pleural fluid of a patient in relapse following chemotherapy and radiotherapy. Previously, we found that despite relatively low *SASS6* mRNA levels, DMS273 had higher SAS-6 protein expression when compared with other lung cancer cell lines (Hargreaves *et al.*, 2025). Using the DepMap Public 26Q1 Dataset to compare gene transcript abundance with CRISPR-derived gene dependency probability, we found that despite moderately low RNA expression, DMS273 was predicted to have a high probability of dependency on *SASS6* (Fig. 1A).

To investigate how SAS-6 could affect cell movement, *SASS6* was targeted with short hairpin RNA (shRNA) in DMS273 cells. shRNA targeting luciferase (not expressed in mammalian genomes) was used as a control (shLuc). SAS-6 depletion was confirmed by western blot (Fig. 1B, 1C, 1D) and by immunostaining (Fig. 1E). Western blot analysis showed the presence of two bands (Fig. 1B) with a marked decrease seen in the top band found at the expected size for SAS-6. Densitometry quantification of either the top band alone or of both bands showed significant SAS-6 reduction following shRNA transduction (Fig. 1C, 1D). Centrin (CETN3) and CP110 staining showed mild centriole amplification in DMS273 cells, which was reduced upon SAS-6 knockdown (Supplementary Fig. 1A, 1B, 1C). The percentage of centrioles with SAS-6 signal was significantly reduced in cells transduced with *SASS6*-targeting shRNA (Fig. 1E, 1F).

SAS-6 localisation at the base of the cilium could be observed in control cells (shLuc) but not in SAS-6 depleted cells (shSASS6) (Fig. 1E), which showed reduced ciliation (Fig. 1E, 1G, 1H). Cilia were visualised clearly with Arl13B, a marker for the ciliary membrane (Fig. 1G), and with detyrosinated tubulin, a posttranslational modification in ciliary microtubules (Fig. 1E), but not with acetylated tubulin, which had a weaker signal, suggesting a distinct tubulin code for these cells (Janke & Magiera, 2020) (Fig. 1G).

As cilia have been shown to integrate signalling pathways that regulate cell migration and metastasis (Collinson & Tanos, 2025) and to promote cellular events required for the successful survival of cancer cells (Légaré *et al.*, 2017, Wang *et al.*, 2017, Jenks *et al.*, 2018, Iruzubieta *et al.*, 2021, Hargreaves *et al.*, 2025), our models of SAS-6 downregulation (DMS273) and overexpression (RPE-1 SAS-6ND) (Hargreaves *et al.*, 2025) represent robust cellular systems to study the role of centrioles and cilia in metastasis.

SAS-6 regulates cell migration in cell-derived matrices

Cell migration is a critical stage in cancer metastasis, required for cells to detach from the primary tumour mass and enter circulation. We have previously shown that SAS-6 overexpression increased cellular invasion in multiple cell lines, and that depleting SAS-6 in SCLC cells with high SAS-6 reduced their ability to invade through a collagen matrix (Hargreaves *et al.*, 2025). Next, we wanted to understand whether SAS-6 might have a role in cell migration in a more physiological setting. For this, we produced 3D cell-derived matrices (CDMs) following the method developed by the Yamada laboratory (Cukierman *et al.*, 2001, Bass *et al.*, 2007). Briefly, telomerase-immortalised fibroblasts (TIFs) were allowed to grow at high density for 8 days in the presence of ascorbic acid to enhance matrix fibril stability. The resulting matrix was then denuded with extraction buffer before cells of interest were seeded on top (Fig. 2A). Compared to commercial matrices such as Matrigel or collagen, CDMs represent a more physiologically relevant tool to examine cell movement and the interaction between cells and ECM. CDMs contain fibrillar proteins, adhesive molecules, growth factors and gel-like molecules, such as proteoglycans and hyaluronic acid and are topographically heterogeneous, closely mimicking in vivo conditions (Kutys *et al.*, 2013).

To track cell migration, control DMS273 and SAS-6 knockdown cells were seeded onto CDMs and imaged for 16 h at 10 min intervals (Fig. 2B, 2C, 2D) (Additional file 1, 2). SAS-6 depletion significantly reduced the average speed of DMS273 cells migrating through matrices compared to controls (Fig. 2H). SAS-6-depleted cells travelled a shorter distance (Fig. 2I) and showed a rounded morphology when compared to the more elongated control cells (Fig. 2B top panels). Conversely, overexpressing SAS-6 with our previously described doxycycline-inducible non-degradable SAS-6 mutant (Myc-tagged SAS-6ND) in RPE-1 cells (Hargreaves *et al.*, 2025) resulted in increased velocity and longer distance travelled in CDMs (Fig. 2E, 2F, 2G, 2J, 2K) (Additional file 3, 4).

Taken together, these data show that SAS-6 perturbation has significant effects on cell migration in different cell types, with increased expression levels correlating with faster migration speed and longer distances.

SAS-6 depletion affects cell morphology and attachment

When tracking DMS273 migration in CDMs, we observed a change in morphology in the SAS-6-depleted cells, which appeared to remain more separated from neighbouring cells throughout the 16 h period (Fig. 2B). To investigate this further, we stained control and SAS-6-depleted DMS273 cells grown in CDMs with phalloidin to visualise any differences in F-actin and overall cell morphology (Fig. 3A). While control cells were arranged in tight clusters of cells with weak actin fibre formation, SAS-6-depleted cells were found to be more spatially disperse across the field of view with more cells showing strong actin stress fibre formation (Fig. 3A).

To understand whether the observed migration defects in SAS-6-depleted cells could be related to changes in their attachment to substrates, we carried out a fibronectin spreading experiment (Kawai *et al.*, 2009). Similarly to what was observed in CDM migration experiments, fibronectin attachment took considerably longer in DMS273 cells, requiring approximately 20 h after seeding before differences in the early stages of attachment became apparent. (Fig. 3B). On fibronectin, DMS273 cells depleted of SAS-6 showed a more spread morphology and displayed more actin stress fibre formation as compared to the controls, mimicking what was observed upon SAS-6 downregulation in cells seeded in CDMs (Figs. 3A, 3B). SAS-6-depleted-cells showed a surface area significantly larger than the controls and a lower form factor, indicating that they are less circular (Figs. 3C, 3D). Staining these cells for vinculin, a component of focal adhesions, showed that SAS-6-depleted cells had higher number of focal adhesions and increased focal adhesion size compared to control cells (Figs. 3E, 3F).

To investigate the impact of SAS-6 overexpression on cell adherence, RPE-1 SAS-6ND cells were induced with doxycycline and also seeded onto fibronectin-coated coverslips (Fig. 3G). As RPE-1 cells attach at a faster rate than DMS273, these were allowed to attach only for 2 h before fixation. An increase in SAS-6 expression was also found to increase cell size (Fig. 3H), perhaps suggesting that dysregulated SAS-6 levels might destabilise the control of cell size and the organisation of the cytoskeleton.

SAS-6 depletion disrupts front-rear polarity

To further assess cell morphology changes upon SAS-6 depletion, DMS273 shLuc and shSASS6 were labelled with the fluorescent actin-binding probe Lifeact-RFP to enable live imaging. Cells were seeded onto CDMs, imaged for 1 h at 2 min intervals, and then analysed using the FIJI plugin ADAPT to quantify cell morphology and membrane dynamics (Fig. 4A) (Additional file 5, 6) (Barry *et al.*, 2015). Regions of membrane protrusion (shown in orange) and retraction (shown in blue) could be visualised for each cell, revealing that control cells showed a defined front-rear polarity with intense areas of actin polymerisation seen at areas of membrane protrusion. In contrast, SAS-6-depleted cells showed a lack of front-rear polarity, as membrane protrusion and retraction were not coordinated to defined leading/rear edges. Actin organisation did not appear to be localised to areas of membrane protrusion, instead showing stress fibre formation across the entire cell.

Interestingly, membrane protrusion and retraction velocities appeared to be slightly increased in SAS-6-depleted cells compared to control cells (Figs. 4B, 4C). However, when looking at the trajectories of the tracked cells over an hour, SAS-6-depleted cells displayed reduced displacement from their point of origin compared to control cells (Fig. 4D), consistent with our results tracking these cells over 16 h (Figs. 2B, 2I). SAS-6 knockdown was confirmed to have remained consistent in the Lifeact-RFP-labelled cells (Figs. 4H, 4I). Our results suggested that despite increased membrane remodelling, SAS-6-depleted cells showed reduced migration in CDMs (Fig. 2B, 2H, 2I). This might be indicative of changes in focal adhesions, as well as a general defect in anterior-posterior polarity (Elric & Etienne-Manneville, 2014). Staining of Lifeact-RFP-expressing cells for vinculin within the CDMs showed an increased number of focal adhesions in SAS-6-depleted cells relative to the shLuc control (Fig. 4E, 4F). However, these focal adhesions distributed along the entire cell perimeter, compared to control cells that showed focal adhesion enrichment at the leading edge of the cell (Fig. 4E). SAS-6-depleted cells also showed an increased number of focal adhesions under the nucleus compared to control cells (Fig. 4E, 4G), which may contribute to the overall reduced migratory capacity of these cells. Thus, a disorganised anterior-posterior polarity and increased attachment to the cell matrix seem to suppress migration in SAS-6-depleted cells.

A coordinated function of SAS-6 with junctional proteins

SAS-6 depleted cells seemed to grow more spatially separated compared to the tightly organised distribution of control cells, suggesting that cell junctions might be less stable (Fig. 3A). Curated interaction data from BioGRID shows that SAS-6 is reported to interact with proteins found to localise at tight junctions (TJP1) and adherens junctions (ABI2 and APC) (Additional file 7) (Grove *et al.*, 2004, Harris & Nelson, 2010, Gupta *et al.*, 2015, Huttlin *et al.*, 2017, Go *et al.*, 2021, Oughtred *et al.*, 2021). Using DepMap's predictability model, we found that many genes involved in cytoskeleton remodelling and cell junction formation were associated with *SASS6* dependence in a pan-cancer analysis (Fig. 5A). Among these genes, *TJP1* was highlighted as one of the genomic features most strongly associated with *SASS6* dependence. Given that TJP1 appeared in both the DepMap and BioGRID analyses, this warranted further investigation. *TJP1* encodes for ZO-1 (Zonula Occludens-1), a critical factor securing tight junction stability (Van Itallie *et al.*, 2009).

Depletion of SAS-6 in DMS273 cells was found to reduce the expression of ZO-1 compared to controls (Figs. 5B, 5C). SAS-6-depleted cells showed disrupted tight junctions, with patchy, discontinuous ZO-1 staining (Fig. 5D). A quantification of the levels and distribution of ZO-1 protein at cell junctions showed a significant reduction in ZO-1 intensity and total ZO-1 area in SAS-6-depleted cells (Figs. 5E, 5F). These results suggest that SAS-6 might cooperate with junctional proteins to promote cell movement.

Discussion

Cancer metastasis is the major cause of cancer-related deaths. One of the key stages in metastasis is migration, when cells move away from the site of origin prior to entering circulation (Hanahan & Weinberg, 2011). Cell migration requires directionality, cell movement, and interactions with the extracellular matrix (Shellard & Mayor, 2020). Therefore, understanding the mechanisms driving cancer cell migration is essential for developing prognostic markers and identifying therapeutic targets. Here we show that SAS-6 promotes cell migration in physiologically relevant cell-derived matrices. Removal of SAS-6 in a metastatic SCLC cell line significantly reduces cell migration and disrupts anterior-posterior polarity during cell movement. Conversely, SAS-6 overexpression increases cell migration in CDMs. SAS-6-depleted cells show significant changes in cell morphology, focal adhesion number and distribution, and cell junction integrity.

Centrosomes and cilia have been shown to function in cell migration (Elric & Etienne-Manneville, 2014, Hargreaves *et al.*, 2025), but the specific regulation of this process is not understood. In immune cells, centriole depletion can increase migration speed in neutrophils (Klemm *et al.*, 2021) yet reduce migration velocity (net movement) and persistence in dendritic cells (Weier *et al.*, 2022). Despite these differences, possibly explained by intrinsic cell-type-specific features, this indicates that directionality driven by anterior-posterior polarity is likely affected in these cells, which is consistent with our findings. Another study found that depletion of SAS-6 in a p53 null background disrupted anterior-posterior polarity and increased number and stability of focal adhesions (Cheng *et al.*, 2019). In this case, a complete SAS-6 knockout rendered cells to be acentriolar, with multiple microtubule organising centres and increased Rac activation that could drive invasion (Cheng *et al.*, 2019). Although Cheng et al observed increased cell movement in SAS-6-null cells, this might be due to the release of a p53-dependent brake to cell migration (Moskovits *et al.*, 2006, Muller *et al.*, 2011) or substrate-specific characteristics. Excessive random Rac1 activation at the cell periphery might help to explain the lack of coordination observed in our membrane dynamics analysis in SAS-6-depleted cells, which did not display a clear leading edge.

SAS-6 depletion increased focal adhesion number and area. Biochemically, SAS-6 has been shown to interact with FAM21, a component of the WASH complex, which functions at the centrosomes to activate the Arp2/3 complex (Farina *et al.*, 2016). Interestingly, the Arp2/3 complex also binds vinculin and focal adhesion kinase at focal adhesions (DeMali *et al.*, 2002). Thus, SAS-6 could function as an organiser at centrioles, leading to changes in the actin cytoskeleton and focal adhesions. In DMS273 cells, SAS-6 is found in basal bodies, similarly to its localisation in motile cilia (Vladar & Stearns, 2007). In multiciliated cells, with motile cilia, focal adhesion proteins such as paxillin, vinculin, and focal adhesion kinase (FAK)

have been described to associate with basal body structures described as ciliary adhesion complexes, anchoring basal bodies to the actin cytoskeleton (Antoniades *et al.*, 2014, Chatzifrangkeskou & Skourides, 2022). Perhaps SAS-6 depletion destabilises the crosstalk between basal bodies and focal adhesion proteins, resulting in cytoskeletal defects.

In addition to changes in cell-matrix adhesion, SAS-6 depletion reduced cell-cell junction formation and expression of the tight junction protein ZO-1. Proximity-label-MS evidence shows that SAS-6 and ZO-1 are likely to physically interact (Gupta *et al.*, 2015). Intriguingly the effects we observe upon SAS-6 knockdown appear to phenocopy the effects of ZO-1 depletion, where cells are observed to have thicker and more elongated focal adhesions (Haas *et al.*, 2022). The authors of that study describe that ZO-1 functions to control cytoskeletal tension and the effects this has on the forces acting on cell-matrix and cell-cell adhesions, closely describing what we observe upon SAS-6 knockdown. ZO-1 has also been described to play an important role in collective cell migration (Park *et al.*, 2024, Hirano *et al.*, 2026), which appears to be how DMS273 cells migrate under normal conditions. Therefore, SAS-6 and ZO-1 could be acting in coordination to maintain the correct balance of cell-matrix adhesion and promote cell migration. How SAS-6 depletion could cause a decrease in total ZO-1 expression is an interesting question which remains to be answered.

Here we show that SAS-6 controls cell migration in RPE-1 cells and metastatic SCLC DMS273 cells, having significant effects on cell adhesion and junction formation. The use of 3D cell-derived matrices (CDMs) in this study provides an important and physiologically relevant matrix for the investigation of cell migration, which will be a useful tool to test the role of SAS-6 in invasion in additional cellular models and cancer types, including lung adenocarcinoma, breast cancer, and colorectal cancer, all known to have high endogenous SAS-6 expression (Shinmura *et al.*, 2015, Du *et al.*, 2021, Li *et al.*, 2024).

Conclusions

This study reveals a role of the centriolar protein SAS-6 in regulating cell migration and cell contacts with the surrounding matrix and other cells. Depletion of SAS-6 was found to reduce migration of lung cancer cells, increase the number of focal adhesions, and resulted in weaker cell junctions with reduced ZO-1. Our work highlights SAS-6 as a promising target to investigate in the context of cancer cell metastasis.

Abbreviations

APC/C-Cdh1
Anaphase-promoting complex/cyclosome-cdc20 homolog 1
CDM
Cell-derived matrix
CP110
Centriolar coiled coil protein 110kDa
ECM

Extracellular matrix

FAK

Focal adhesion kinase

MTOC

Microtubule organising centre

RFP

Red fluorescent protein

SAS-6/SASS6

Spindle assembly abnormal protein 6 homolog

SAS-6ND

SAS-6-nondegradable

SCLC

Small cell lung cancer

shRNA

Short hairpin RNA

STIL

SCL-interrupting locus protein

TAZ

Transcriptional co-activator with PDZ-binding motif

TJP1

Tight junction protein-1

YAP

Yes-associated protein

ZO-1

Zonula occludens-1

Declarations

Acknowledgements

We would like to acknowledge members of the Biosciences technical team and all our colleagues at Brunel University of London for their support with this work. We would also like to thank Natalia Castro Mena for her assistance with cell sorting. We are grateful to Igor Vivanco (Kings College London) and Naoko Kogata (Way lab, The Francis Crick Institute) for providing cell lines and reagents. We thank Igor Vivanco (King's College London), Fernando Calvo (Universidad de Cantabria) and Pedro Monteiro (Barts Cancer Institute, QMUL) for critically reading this manuscript.

Funding

This work was supported by a June Hancock Mesothelioma Research Fund (JH-21-14) and a Kidney Research UK Senior Fellowship (SF_002_20220706) to BT and by Brunel University of London.

Author information

Authors and affiliations

Laboratory of Centriole & Cilia Biogenesis, Signaling and Function, Department of Biosciences, College of Health, Medicine and Life Sciences, Brunel University London, Kingston Lane, London, UB8 3PH, United Kingdom.

Rebecca Collinson, Zoi Grigoriou-Mirallais, Barbara Tanos

Centre for Genome Engineering and Maintenance, College of Health, Medicine and Life Sciences, Brunel University London, Kingston Lane, London, UB8 3PH, United Kingdom.

Rebecca Collinson, Zoi Grigoriou-Mirallais, Elizabeth McCarthy, Joseph Hetmanski, Barbara Tanos

Contributions

B.T. and R.C. conceptualised the study. B.T., R.C, J.H, and E.M. developed the methodology. R.C., B.T., and J.H. carried out data analysis and interpretation. R.C., Z.G.-M., J.H. and E.M. conducted experiments. B.T and J.H provided resources and supervision. B.T. provided funding. R.C. and B.T. wrote the original draft. B.T., R.C, and J.H. reviewed and edited the manuscript.

Corresponding author

Correspondence to Barbara Tanos.

Ethics declarations

Competing interests

The authors declare that they have no financial or non-financial competing interests.

Ethics approval and consent to participate

Not applicable.

References

1. Antoniades I, Stylianou P & Skourides PA (2014) Making the connection: ciliary adhesion complexes anchor basal bodies to the actin cytoskeleton. *Dev Cell* **28**: 70–80.
2. Appert-Collin A, Bennasroune A, Jeannesson P, Terryn C, Fuhrmann G, Morjani H & Dedieu S (2017) Role of LRP-1 in cancer cell migration in 3-dimensional collagen matrix. *Cell Adh Migr* **11**: 316–326.
3. Arafeh R, Shibue T, Dempster JM, Hahn WC & Vazquez F (2025) The present and future of the Cancer Dependency Map. *Nature Reviews Cancer* **25**: 59–73.

4. Barry DJ, Durkin CH, Abella JV & Way M (2015) Open source software for quantification of cell migration, protrusions, and fluorescence intensities. *Journal of Cell Biology* **209**: 163–180.
5. Bass MD, Roach KA, Morgan MR, Mostafavi-Pour Z, Schoen T, Muramatsu T, Mayer U, Ballestrem C, Spatz JP & Humphries MJ (2007) Syndecan-4-dependent Rac1 regulation determines directional migration in response to the extracellular matrix. *J Cell Biol* **177**: 527–538.
6. Chatzifrangkeskou M & Skourides PA (2022) The apical ciliary adhesion complex is established at the basal foot of motile cilia and depends on the microtubule network. *Scientific Reports* **12**: 19028.
7. Cheng H-W, Hsiao C-T, Chen Y-Q, Huang C-M, Chan S-I, Chiou A & Kuo J-C (2019) Centrosome guides spatial activation of Rac to control cell polarization and directed cell migration. *Life Science Alliance* **2**: e201800135.
8. Collinson R & Tanos B (2025) Primary cilia and cancer: a tale of many faces. *Oncogene* **44**: 1551–1566.
9. Cukierman E, Pankov R, Stevens DR & Yamada KM (2001) Taking cell-matrix adhesions to the third dimension. *Science* **294**: 1708–1712.
10. Delattre M, Canard C & Gönczy P (2006) Sequential protein recruitment in C. elegans centriole formation. *Curr Biol* **16**: 1844–1849.
11. DeMali KA, Barlow CA & Burridge K (2002) Recruitment of the Arp2/3 complex to vinculin: coupling membrane protrusion to matrix adhesion. *J Cell Biol* **159**: 881–891.
12. Dillekås H, Rogers MS & Straume O (2019) Are 90% of deaths from cancer caused by metastases? *Cancer Med* **8**: 5574–5576.
13. Du L, Jing J, Wang Y, *et al.* (2021) Knockdown of SASS6 reduces growth of MDA-MB-231 triple-negative breast cancer cells through arrest of the cell cycle at the G2/M phase. *Oncol Rep* **45**.
14. Elric J & Etienne-Manneville S (2014) Centrosome positioning in polarized cells: common themes and variations. *Exp Cell Res* **328**: 240–248.
15. Farina F, Gaillard J, Guérin C, Couté Y, Sillibourne J, Blanchoin L & Théry M (2016) The centrosome is an actin-organizing centre. *Nat Cell Biol* **18**: 65–75.
16. Go CD, Knight JDR, Rajasekharan A, *et al.* (2021) A proximity-dependent biotinylation map of a human cell. *Nature* **595**: 120–124.
17. Godinho SA & Pellman D (2014) Causes and consequences of centrosome abnormalities in cancer. *Philos Trans R Soc Lond B Biol Sci* **369**.
18. Godinho SA, Picone R, Burute M, Dagher R, Su Y, Leung CT, Polyak K, Brugge JS, Théry M & Pellman D (2014) Oncogene-like induction of cellular invasion from centrosome amplification. *Nature* **510**: 167–171.
19. Grove M, Demyanenko G, Echarri A, *et al.* (2004) ABI2-deficient mice exhibit defective cell migration, aberrant dendritic spine morphogenesis, and deficits in learning and memory. *Mol Cell Biol* **24**: 10905–10922.

20. Gupta GD, Coyaud É, Gonçalves J, *et al.* (2015) A Dynamic Protein Interaction Landscape of the Human Centrosome-Cilium Interface. *Cell* **163**: 1484–1499.
21. Haas AJ, Zihni C, Krug SM, Maraspini R, Otani T, Furuse M, Honigmann A, Balda MS & Matter K (2022) ZO-1 Guides Tight Junction Assembly and Epithelial Morphogenesis via Cytoskeletal Tension-Dependent and -Independent Functions. *Cells* **11**.
22. Hanahan D & Weinberg Robert A (2011) Hallmarks of Cancer: The Next Generation. *Cell* **144**: 646–674.
23. Hargreaves E, Collinson R, Jenks AD, *et al.* (2025) Dysregulated SASS6 expression promotes increased ciliogenesis and cell invasion phenotypes. *Life Sci Alliance* **8**.
24. Harris ES & Nelson WJ (2010) Adenomatous polyposis coli regulates endothelial cell migration independent of roles in beta-catenin signaling and cell-cell adhesion. *Mol Biol Cell* **21**: 2611–2623.
25. Hirano S, Kondo Y, Kitajima A, Kinoshita N, Otani T, Furuse M, Ueno N & Aoki K (2026) ZO-1 shuttles between apical junctional complexes and podosomes by riding ERK activation waves. *Nature Communications* **17**: 6284.
26. Huttlin EL, Bruckner RJ, Paulo JA, *et al.* (2017) Architecture of the human interactome defines protein communities and disease networks. *Nature* **545**: 505–509.
27. Iruzubieta P, Castiella T, Monleón E, Berga C, Muñoz G & Junquera C (2021) Primary cilia presence and implications in bladder cancer progression and invasiveness. *Histochemistry and Cell Biology* **155**: 547–560.
28. Janke C & Magiera MM (2020) The tubulin code and its role in controlling microtubule properties and functions. *Nat Rev Mol Cell Biol* **21**: 307–326.
29. Jenks AD, Vyse S, Wong JP, *et al.* (2018) Primary Cilia Mediate Diverse Kinase Inhibitor Resistance Mechanisms in Cancer. *Cell Rep* **23**: 3042–3055.
30. Kawai K, Iwamae Y, Yamaga M, Kiyota M, Ishii H, Hirata H, Homma Y & Yagisawa H (2009) Focal adhesion-localization of START-GAP1/DLC1 is essential for cell motility and morphology. *Genes to Cells* **14**: 227–241.
31. Klemm LC, Denu RA, Hind LE, Rocha-Gregg BL, Burkard ME, Huttenlocher A & Montell D (2021) Centriole and Golgi microtubule nucleation are dispensable for the migration of human neutrophil-like cells. *Molecular Biology of the Cell* **32**: 1545–1556.
32. Kutys ML, Doyle AD & Yamada KM (2013) Regulation of cell adhesion and migration by cell-derived matrices. *Exp Cell Res* **319**: 2434–2439.
33. Lee MY, Marina M, King JL & Saavedra HI (2014) Differential expression of centrosome regulators in Her2 + breast cancer cells versus non-tumorigenic MCF10A cells. *Cell Div* **9**: 3.
34. Légaré S, Chabot C & Basik M (2017) SPEN, a new player in primary cilia formation and cell migration in breast cancer. *Breast Cancer Research* **19**: 104.
35. Leidel S, Delattre M, Cerutti L, Baumer K & Gönczy P (2005) SAS-6 defines a protein family required for centrosome duplication in C. elegans and in human cells. *Nat Cell Biol* **7**: 115–125.

36. Levine MS, Bakker B, Boeckx B, *et al.* (2017) Centrosome Amplification Is Sufficient to Promote Spontaneous Tumorigenesis in Mammals. *Dev Cell* **40**: 313–322.e315.
37. Li Z, He L, Li J, *et al.* (2024) SASS6 promotes tumor proliferation and is associated with TP53 and immune infiltration in lung adenocarcinoma. *Clin Exp Med* **24**: 243.
38. Marteil G, Guerrero A, Vieira AF, *et al.* (2018) Over-elongation of centrioles in cancer promotes centriole amplification and chromosome missegregation. *Nat Commun* **9**: 1258.
39. Meijering E, Dzyubachyk O & Smal I (2012) Chapter nine - Methods for Cell and Particle Tracking. *Methods in Enzymology*, Vol. 504 (conn PM, ed.) p.^pp. 183–200. Academic Press.
40. Mill P, Christensen ST & Pedersen LB (2023) Primary cilia as dynamic and diverse signalling hubs in development and disease. *Nat Rev Genet* **24**: 421–441.
41. Moskovits N, Kalinkovich A, Bar J, Lapidot T & Oren M (2006) p53 Attenuates Cancer Cell Migration and Invasion through Repression of SDF-1/CXCL12 Expression in Stromal Fibroblasts. *Cancer Research* **66**: 10671–10676.
42. Muller PA, Vousden KH & Norman JC (2011) p53 and its mutants in tumor cell migration and invasion. *J Cell Biol* **192**: 209–218.
43. Oughtred R, Rust J, Chang C, *et al.* (2021) The BioGRID database: A comprehensive biomedical resource of curated protein, genetic, and chemical interactions. *Protein Sci* **30**: 187–200.
44. Park A, Choi S, Do J, Kim Y, Kim KS, Koh E & Park KS (2024) ZO-1 regulates the migration of mesenchymal stem cells in cooperation with α-catenin in response to breast tumor cells. *Cell Death Discov* **10**: 19.
45. Pelletier L, O'Toole E, Schwager A, Hyman AA & Müller-Reichert T (2006) Centriole assembly in Caenorhabditis elegans. *Nature* **444**: 619–623.
46. Satir P & Christensen ST (2007) Overview of structure and function of mammalian cilia. *Annu Rev Physiol* **69**: 377–400.
47. Shellard A & Mayor R (2020) All Roads Lead to Directional Cell Migration. *Trends in Cell Biology* **30**: 852–868.
48. Shinmura K, Kato H, Kawanishi Y, *et al.* (2015) SASS6 overexpression is associated with mitotic chromosomal abnormalities and a poor prognosis in patients with colorectal cancer. *Oncol Rep* **34**: 727–738.
49. Stirling DR, Swain-Bowden MJ, Lucas AM, Carpenter AE, Cimini BA & Goodman A (2021) CellProfiler 4: improvements in speed, utility and usability. *BMC Bioinformatics* **22**: 433.
50. Strnad P, Leidel S, Vinogradova T, Euteneuer U, Khodjakov A & Gönczy P (2007) Regulated HsSAS-6 Levels Ensure Formation of a Single Procentriole per Centriole during the Centrosome Duplication Cycle. *Developmental Cell* **13**: 203–213.
51. Sugioka K, Hamill DR, Lowry JB, McNeely ME, Enrick M, Richter AC, Kiebler LE, Priess JR & Bowerman B (2017) Centriolar SAS-7 acts upstream of SPD-2 to regulate centriole assembly and pericentriolar material formation. *Elife* **6**.

52. Ueda M, Gräf R, MacWilliams HK, Schliwa M & Euteneuer U (1997) Centrosome positioning and directionality of cell movements. *Proc Natl Acad Sci U S A* **94**: 9674–9678.
53. Van Itallie CM, Fanning AS, Bridges A & Anderson JM (2009) ZO-1 stabilizes the tight junction solute barrier through coupling to the perijunctional cytoskeleton. *Mol Biol Cell* **20**: 3930–3940.
54. Vladar EK & Stearns T (2007) Molecular characterization of centriole assembly in ciliated epithelial cells. *J Cell Biol* **178**: 31–42.
55. Wang CY, Tsai HL, Syu JS, Chen TY & Su MT (2017) Primary Cilium-Regulated EG-VEGF Signaling Facilitates Trophoblast Invasion. *J Cell Physiol* **232**: 1467–1477.
56. Weier A-K, Homrich M, Ebbinghaus S, *et al.* (2022) Multiple centrosomes enhance migration and immune cell effector functions of mature dendritic cells. *Journal of Cell Biology* **221**.
57. Xu Y, Zhu K, Chen J, Lin L, Huang Z, Zhang J & Chen Y (2021) SASS6 promotes proliferation of esophageal squamous carcinoma cells by inhibiting the p53 signaling pathway. *Carcinogenesis* **42**: 254–262.
58. Yamada KM & Cukierman E (2007) Modeling tissue morphogenesis and cancer in 3D. *Cell* **130**: 601–610.
59. Zhang J & Wang YL (2017) Centrosome defines the rear of cells during mesenchymal migration. *Mol Biol Cell* **28**: 3240–3251.
60. Zhang J, Guo WH & Wang YL (2014) Microtubules stabilize cell polarity by localizing rear signals. *Proc Natl Acad Sci U S A* **111**: 16383–16388.

Figures

Figure 1

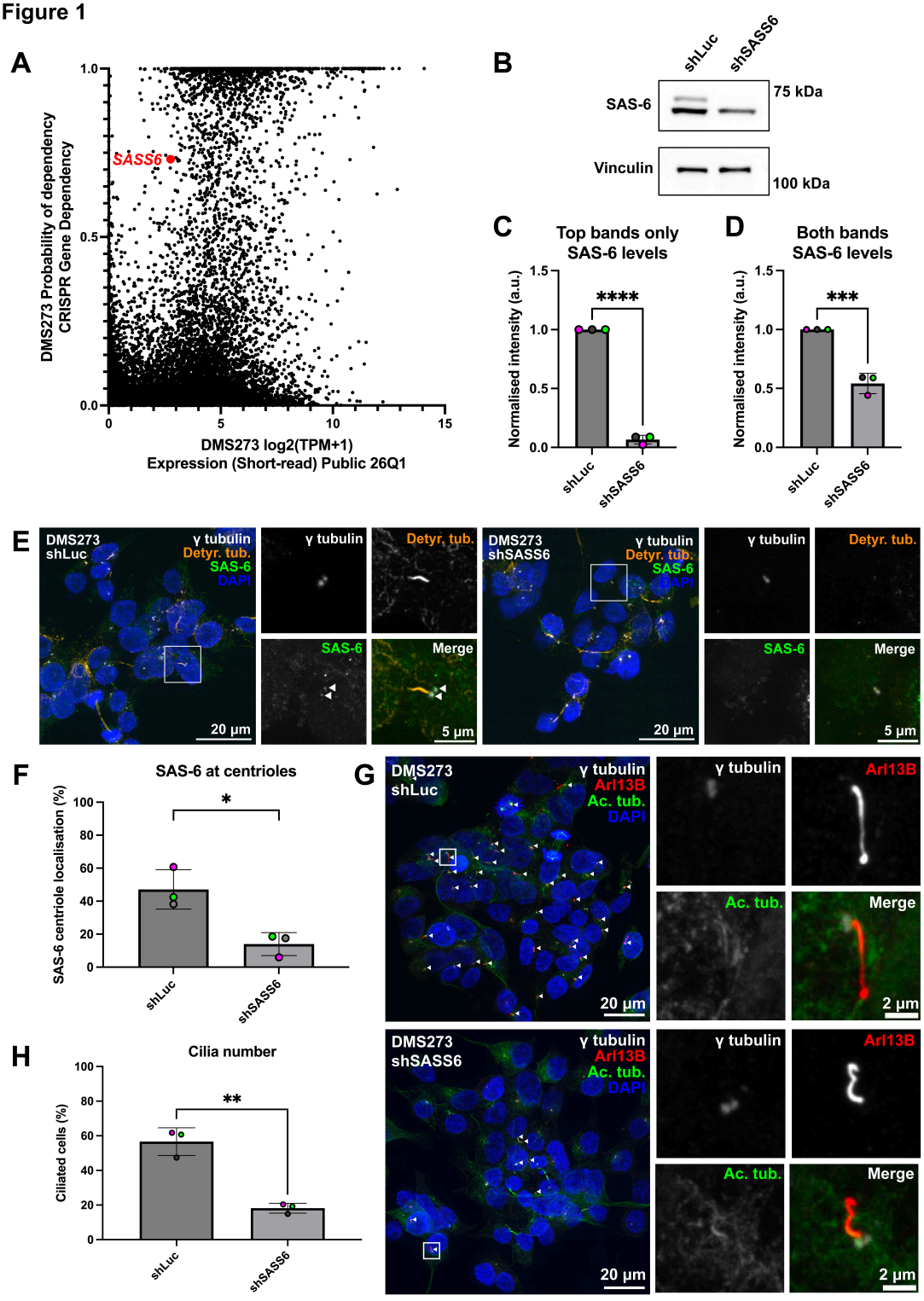


Figure 1

Characterisation of a ciliated metastatic cancer cell line to study cell migration. A) Plot using available DepMap data showing gene dependency probability estimates versus mRNA expression (DepMap Public 26Q1, log2[TPM+1]) in DMS273, with *SASS6* highlighted in red. **B)** Western blot showing expression of SAS-6 in DMS273 shLuc and shSASS6. Vinculin was used as a loading control. Blot is representative of three repeats. **C)** Densitometric quantification of SAS-6 (upper band only) relative to the loading control.

D) Densitometric quantification of SAS-6 (both observed bands) relative to the loading control. **E)** Representative images of DMS273 shLuc and shSASS6. Cells are stained for cilia (detyrosinated tubulin; orange), centrioles (g-tubulin; white), and SAS-6 (green). DNA is marked with DAPI (blue). **F)** Quantification of centrioles with SAS-6 localisation in DMS273 shLuc and shSASS6 cells. n > 400 cells analysed across N = 3 repeats. **G)** Representative images of DMS273 shLuc and shSASS6. Cells are stained for ciliary markers acetylated tubulin (green) and Arl13B (red), and centriole marker g-tubulin (white). DNA is marked with DAPI (blue). **H)** Quantification of cilia number (percent) in DMS273 shLuc and shSASS6. n > 400 cells analysed across N = 3 repeats.

****p < 0.0001, ***p < 0.001, **p < 0.01, *p < 0.05. Unpaired t-tests were performed in C, D, F, and H. Error bars represent standard deviation.

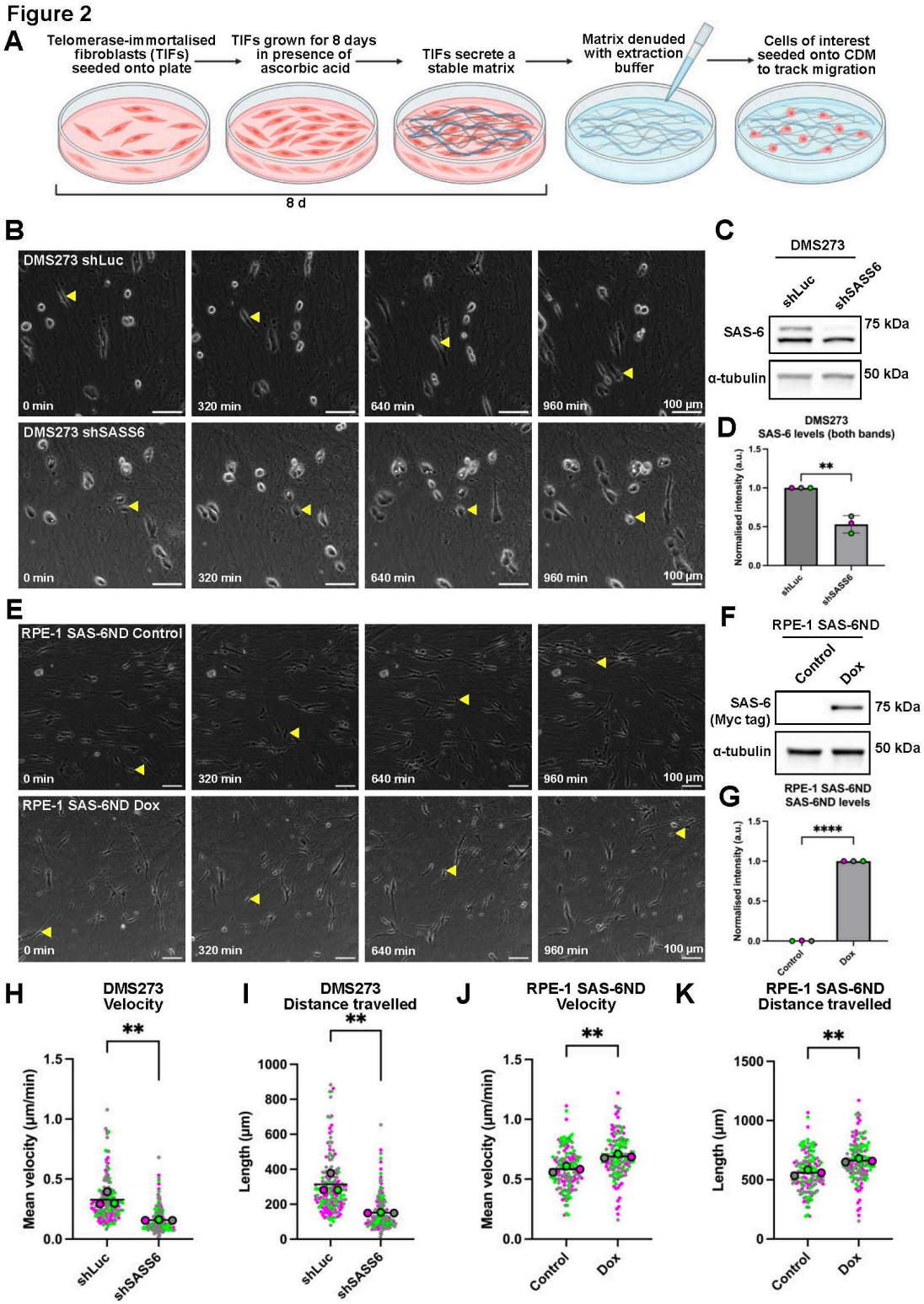


Figure 2

SAS-6 regulates cell migration across cell-derived matrices (CDMs). A) Schematic showing the production of 3D CDMs by telomerase-immortalised fibroblasts (TIFs) over 8 d. **B)** Control and SAS-6-depleted DMS273 cells migrating in CDM over 16 h. Yellow arrowheads indicate the same cell across the 16 h period. **C)** Western blot showing expression of SAS-6 in DMS273 cells transfected with shLuc and shSASS6. a-tubulin is used as a loading control. Blot is representative of three repeats. **D)** Densitometric

quantification of SAS-6 expression (both bands) relative to the loading control. **E)** Control and doxycycline-treated RPE-1 SAS-6ND cells migrating in CDM over 16 h. Yellow arrowheads indicate the same cell across the 16 h period. **F)** Western blot showing expression of Myc-tagged SAS-6ND. a-tubulin is used as a loading control. Blot is representative of three repeats. **G)** Densitometric quantification of SAS-6ND in RPE-1 SAS-6ND cells treated with and without doxycycline, relative to the loading control. **H)** Average migration velocity (μm/min) of DMS273 shLuc and shSASS6 cells over 16 h. n = 175 cells across N = 3 biological replicates. **I)** Average distance travelled (μm) over 16 h by DMS273 shLuc and shSASS6 cells. n = 175 cells across N = 3 biological replicates. **J)** Average migration velocity (μm/min) of RPE-1 SAS-6ND cells over 16 h. n = 140 cells across N = 3 biological replicates. **K)** Average distance travelled (μm) over 16 h by RPE-1 SAS-6ND cells. n = 140 cells across N = 3 biological replicates.

****p < 0.0001, **p < 0.01. Unpaired t-tests were performed in D, G, H, I, J, and K. Error bars represent standard deviation.

Figure 3

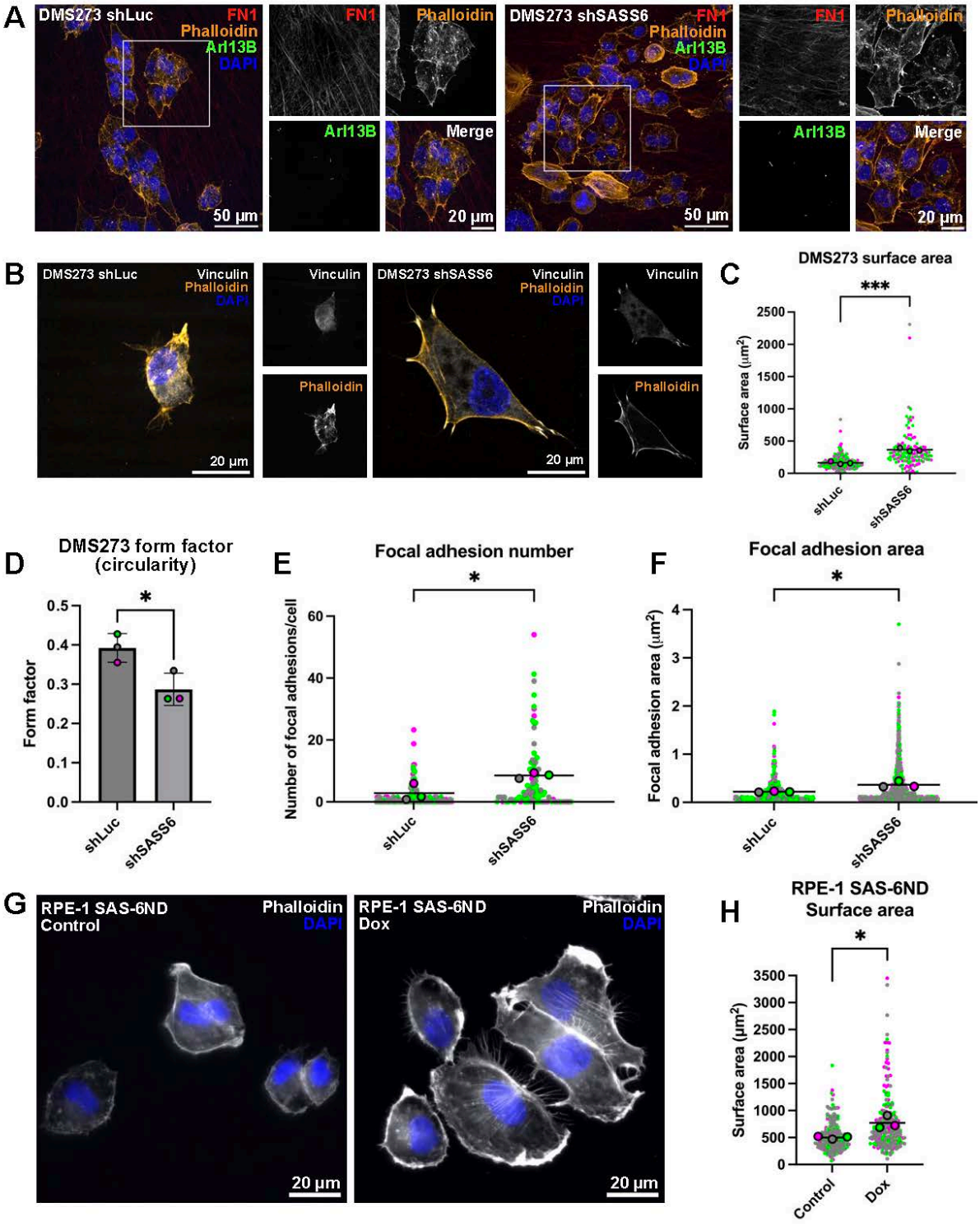


Figure 3

Dysregulated SAS-6 levels cause distinct changes in cell morphology. A) Representative images of DMS273 shLuc and shSASS6 cells growing in 3D CDMs. Cells are stained for F-actin (phalloidin; orange) and cilia (Arl13B; green). CDM is marked with FN1 (red), and DNA is marked with DAPI (blue). **B)** Representative images of DMS273 shLuc and shSASS6 cells growing on FN-coated coverslips 20 h after seeding. Cells are stained for focal adhesions (vinculin; white) and F-actin (phalloidin; orange). DNA is

marked with DAPI (blue). **C, D, E, F)** Quantification of the surface area (C), form factor (D), focal adhesion number (E), and focal adhesion size (F) of DMS273 shLuc and shSASS6 cells grown on FN-coated coverslips. n > 125 cells analysed across N = 3 repeats. **G)** Representative images of RPE-1 SAS-6ND cells in the absence and presence of doxycycline 4 h after seeding onto FN-coated coverslips. Cells are stained for F-actin (phalloidin; white) and DNA is marked with DAPI (blue). **H)** Quantification of surface area of RPE-1 SAS-6ND control and dox cells allowed to spread on FN-coated coverslips for 2 h. n > 225 cells analysed across N = 3 repeats

***p < 0.001, **p < 0.01, *p < 0.05. Unpaired t-tests were performed in C, D, E, F, and H. Error bars represent standard deviation.

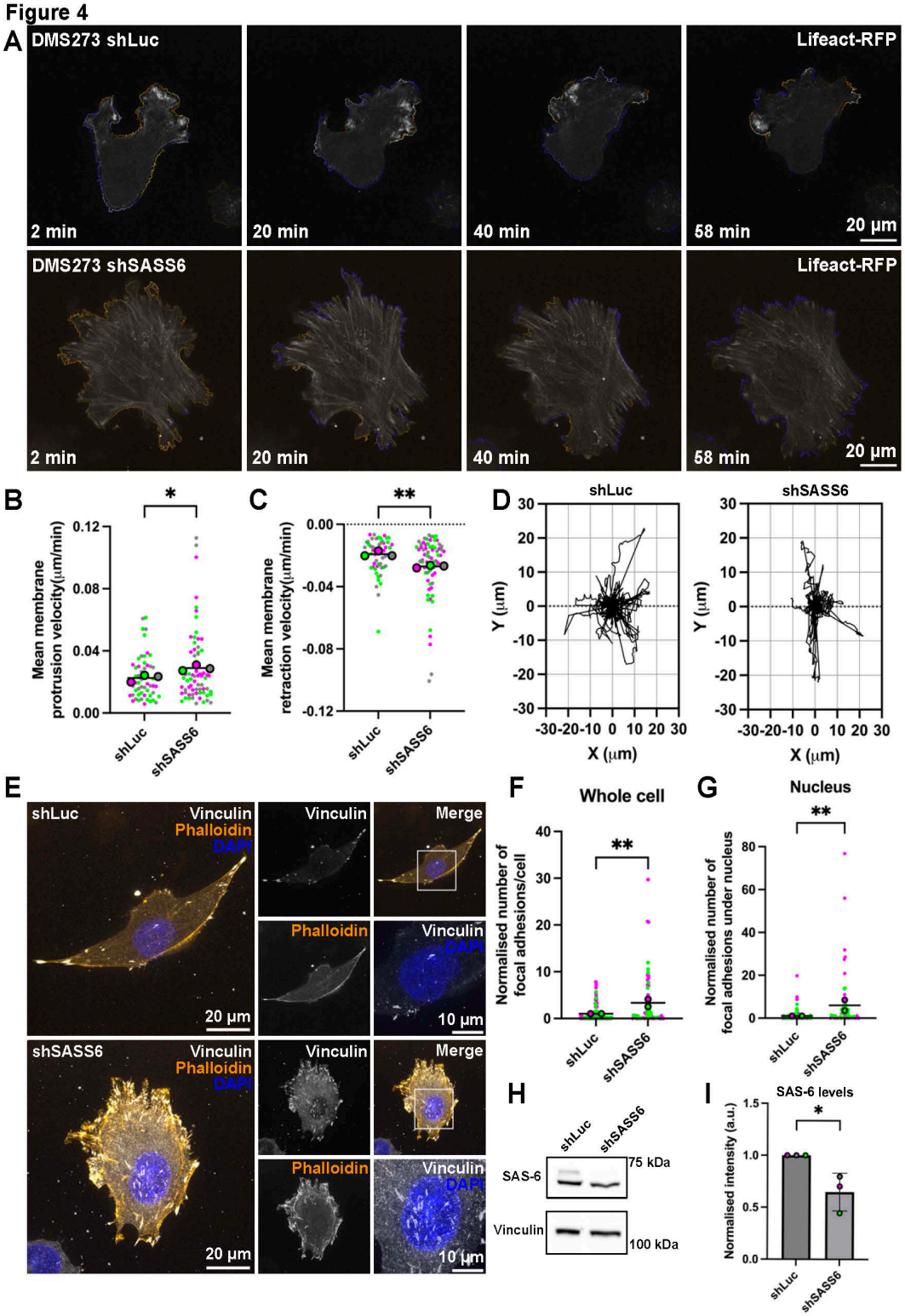


Figure 4

SAS-6 depletion disrupts front-rear polarity. A) Representative images of DMS273 shLuc and shSASS6 cells expressing Lifeact-RFP (white) growing on CDMs. Cells were imaged every 2 min for a total of 1 h. Cell membrane dynamics were analysed using ADAPT, with regions of membrane protrusion shown in orange and regions of membrane retraction shown in blue. **B, C)** Quantification of mean membrane protrusion **(B)** and retraction **(C)** velocities per cell. n > 50 cells across N = 3 repeats **D)** Plots showing

the trajectories of shLuc and shSASS6 cells relative to their point of origin across the 1 h. n > 44 cells across N = 2 repeats. **E)** Representative images of Lifeact-RFP-expressing DMS273 shLuc and shSASS6 cells. Cells were stained for focal adhesions (vinculin; white). DNA is marked with DAPI (blue). Magnified view showing vinculin (white) in the region of the nucleus (blue). **F, G)** Quantification of focal adhesion number relative to the shLuc control in the whole cell **(F)** and under the nucleus **(G)**. Focal adhesion number is normalised to the shLuc control to account for intrinsic variability in CDMs between repeats. n > 60 cells analysed across N = 2 repeats. **H)** Western blot showing expression of SAS-6 in DMS273 cells transfected with shLuc and shSASS6. Vinculin is used as a loading control. Blot is representative of three repeats. **I)** Densitometric quantification of SAS-6 expression (both bands) relative to the loading control.

Figure 5

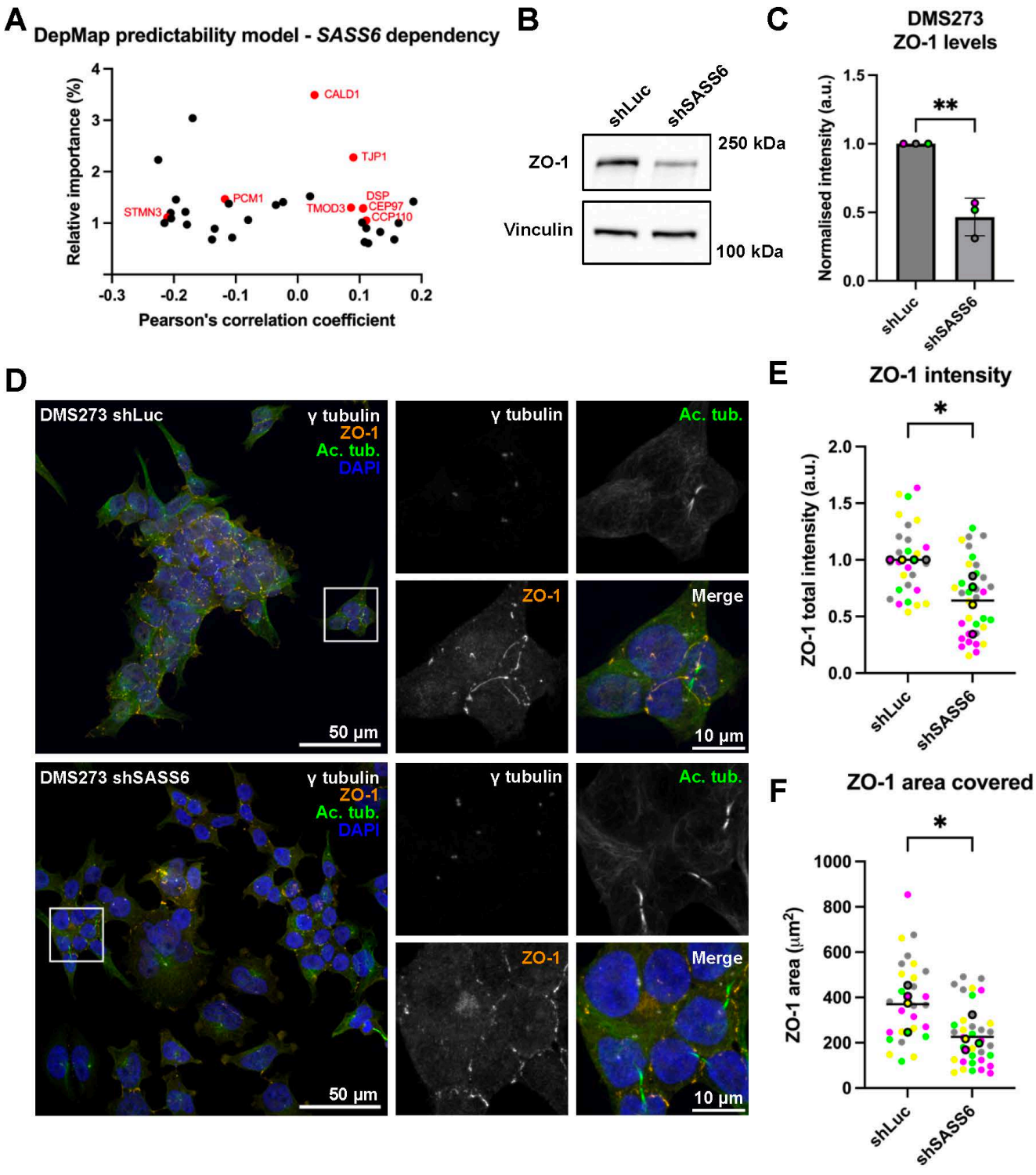


Figure 5

SAS-6 depletion reduces ZO-1 expression and tight junction formation. A) Representation of the DepMap *SASS6* dependence predictability model using CoreOmics features. Genes highlighted in red represent those involved in centrosome, cytoskeleton, and junction organisation. **B)** Western blot showing expression of ZO-1. Vinculin is used as a loading control, blot is representative of three repeats. **C)** Densitometric quantification of ZO-1 in shLuc and shSASS6 DMS273 cells, relative to the loading

control. **D)** Representative images showing shLuc and shSASS6 DMS273 cells. Cells are stained for g-tubulin (white), ZO-1 (orange), and acetylated tubulin (green). DNA is marked with DAPI (blue). **E)** Quantification of ZO-1 intensity at cell junctions in DMS273 shLuc and shSASS6 cells, relative to the shLuc control. N = 4 repeats. **F)** Quantification of total ZO-1-positive cell junction area in DMS273 shLuc and shSASS6 cells. N = 4 repeats.

**p < 0.01, *p < 0.05. Unpaired t-tests were performed in C, E, and F. Error bars represent standard deviation.

Supplementary Files

This is a list of supplementary files associated with this preprint. Click to download.

- Additionalfile1.avi
- Additionalfile2.avi
- Additionalfile3.avi
- Additionalfile4.avi
- Additionalfile5.avi
- Additionalfile6.avi
- Additionalfile7.xlsx
- Supplementarymerged.pdf